Theor. Comput. Fluid Dyn.
DOI 10.1007/s00162-012-0259-9

ORIGINAL ARTICLE

**Sebastian Remmler · Stefan Hickel**

# Spectral structure of stratified turbulence: direct numerical simulations and predictions by large eddy simulation

Received: 1 August 2011 / Accepted: 11 January 2012


**Abstract** Density stratification has a strong impact on turbulence in geophysical flows. Stratification changes the spatial turbulence spectrum and the energy transport and conversion within the spectrum. We analyze these effects based on a series of direct numerical simulations (DNS) of stratified turbulence. To facilitate simulations of real-world problems, which are usually beyond the reach of DNS, we propose a subgrid-scale turbulence model for large eddy simulations of stratified flows based on the Adaptive Local Deconvolution Method (ALDM). Flow spectra and integral quantities predicted by ALDM are in excellent agreement with direct numerical simulation. ALDM automatically adapts to strongly anisotropic turbulence and is thus a suitable tool for studying turbulent flow phenomena in atmosphere and ocean.

**Keywords** Stratified turbulence · Direct numerical simulation · Large eddy simulation · Subgrid-scale modeling

## 1 Introduction

Density stratification is a common situation in geophysical fluid flows that affects turbulence strongly. Stratification suppresses vertical motions typically leading to a $k_v^{-3}$ scaling of the vertical turbulence kinetic energy spectrum, while the horizontal spectrum shows a $k_h^{-5/3}$ inertial range. These different scaling laws render all scales of the velocity field strongly anisotropic, which poses a true challenge for turbulence models and parameterizations.

The horizontal velocity spectrum in the atmosphere was analyzed by Nastrom and Gage [31] using aircraft observations. They found a power-law behavior in the mesoscale range with an exponent of $-5/3$. There has been a long an intensive discussion whether this spectrum is due to a backward cascade of energy [13,16,26] as it is known for two-dimensional turbulence [24], or due to intermittent breaking of internal waves [7,8,36] and thus a forward cascade of energy. In different numerical and theoretical studies, ambiguous or even conflicting results were obtained [27]. Despite this discussion about its origin, the inertial range itself with an exponent of $-5/3$ in the horizontal spectrum has been confirmed by most authors.

During the last decade, a number of new simulations [25,33,38] suggested that the character of the flow depends on the Reynolds number. High Reynolds numbers are associated with stronger three-dimensionality and a forward cascade of energy. Lindborg [28] presented a scaling analysis of the Boussinesq

Communicated by Klein.

S. Remmler (✉) · S. Hickel
Institute of Aerodynamics and Fluid Mechanics, Technische Universität München, 85747 Garching bei München, Germany
E-mail: remmler@tum.de

S. Hickel
E-mail: sh@tum.de

Published online: 02 February 2012

equations for low Froude and high Reynolds number. His theory of strongly anisotropic, but still three-dimensional, turbulence explains the horizontal $k_h^{-5/3}$-spectrum as well as the vertical $k_v^{-3}$-spectrum observed by Cot [6]. On the basis of these findings, Brethouwer et al. [5] showed that the relevant non-dimensional parameter for stratified turbulence is the buoyancy Reynolds number $\mathcal{R} = Fr^2 Re$. For $\mathcal{R} \gg 1$, they predict stratified turbulence including local overturning and a forward energy cascade. In the opposite limit, for $\mathcal{R} \ll 1$, the flow is controlled by viscosity and does not contain small-scale turbulent motions.

Since a full resolution of all turbulence scales is only possible for very low Reynolds numbers, many groups resorted to large eddy simulations (LES) and used subgrid-scale (SGS) models in their computations. For example, Métais and Lesieur [30] used a spectral eddy viscosity model, based on the eddy-damped quasi-normal Markovian (EDQNM) theory. This required a flow simulation in Fourier space and the cut-off wavenumber to be in the inertial range. For classical LES in physical space, Smagorinsky models are widely used, either in the classical formulation [22] or with certain modifications for stratified turbulence based on the local Richardson number [11]. Staquet and Godeferd [35] presented a two-point closure statistical EDQNM turbulence model, which was adapted for axisymmetric spectra about the vertical axis. Recently, many groups presented regularized direct numerical simulations (DNS) of stratified turbulence, which means rather pragmatically stabilizing under-resolved DNS by removing the smallest resolved scales. This is often achieved by a hyperviscosity approach [28,29], which is frequently combined with rigorous de-aliasing in spectral methods using the 2/3-rule [4,12], or by explicit spectral filtering [9].

All explicit SGS turbulence closures for LES suffer from the problem that the computed SGS stresses are of the same order as the grid truncation error. This interference between SGS model and numerical scheme may lead to computational instability and a lack of grid convergence. A possible solution for this issue is a combination of discretization scheme and SGS model in a unified framework. Such approaches are usually referred to as "implicit" LES (ILES) in contrast to the traditional "explicit" SGS models. ILES methods are particularly appealing for the simulation of stratified flows, where the fundamental assumptions of conventional eddy viscosity-based turbulence models may not hold. Several approaches to ILES have been developed in the past, which led to a comprehensive textbook edited by Grinstein et al. [14]. First indications that the truncation error of linear upwind schemes in some cases may function as an implicit SGS model so that no explicit SGS model has to be added to the discretized flow equations were reported by Kawamura and Kuwahara [23]. The use of nonlinearly stable higher-order schemes (i.e., monotonic, monotonicity preserving, or total variation diminishing methods) for so-called Monotonically Integrated LES (MILES) has been proposed by Boris et al. [3]. Particularly noteworthy is the Multidimensional Positive Definite Advection Transport Algorithm (MPDATA) of Smolarkiewicz and Margolin [34], which has been applied widely to geophysical flows. However, when using nonlinearly stable schemes for ILES, one must be aware that most previously proposed methods only guarantee numerical stability, which is necessary, but not sufficient for the physically correct dynamics of the resolved scales. Employing implicit LES for predictive science requires that not only mathematical but also physical constraints have to be incorporated into the design of an implicit SGS model. The first ILES method which is not only based on numerical considerations but also involves physical constraints is the Adaptive Local Deconvolution Method (ALDM) for incompressible neutrally stratified fluids presented by Hickel et al. [19]. Based on this method and ALDM for passive scalar transport [20], we developed an implicit SGS model for Boussinesq fluids.

So far most numerical and experimental studies of stratified turbulence were concentrating on the purely horizontal or vertical spectra of turbulence. In the first part of the present study, we will extend this work and discuss the spatial structure of the turbulence energy spectrum. We shall show how stratification changes the shape of the spectrum with respect to the spherically symmetric spectrum known from isotropic turbulence. Stratified turbulence is called "pancake-turbulence" by several authors, because of the large horizontal and small vertical extension of flow structures in physical space. We will demonstrate how this translates into spectral space as well. Furthermore, we will analyze the contributions of the different terms in the energy transport equation on the total spectral energy balance. This will enable us to follow the flow energy from its injection into the flow through all transport and conversion mechanisms eventually to molecular dissipation.

Based on this detailed analysis of homogeneous stratified turbulence by direct numerical simulation, we will assess the applicability of the implicit SGS model ALDM to this type of flow in the second part of the paper. The comparison of spectra from ALDM simulations with results of DNS and of the standard Smagorinsky model (SSM) will be part of this analysis.

## 2 Governing equations

The non-dimensional Boussinesq equations for a stably stratified fluid in Cartesian coordinates read

$$\nabla \cdot \mathbf{u} = 0 \tag{1a}$$

$$\partial_t \mathbf{u} + \nabla \cdot (\mathbf{u}\mathbf{u}) = -\nabla p - \frac{\rho}{Fr_0^2}\mathbf{e}_z + \frac{1}{Re_0}\nabla^2 \mathbf{u} \tag{1b}$$

$$\partial_t \rho + \nabla \cdot (\rho \mathbf{u}) = \mathbf{u}\mathbf{e}_z + \frac{1}{Pr\ Re_0}\nabla^2 \rho \tag{1c}$$

where velocities are made non-dimensional by $\mathcal{U}$, all spatial coordinates by the length scale $\mathcal{L}$, pressure by $\mathcal{U}^2$, time by $\mathcal{L}/\mathcal{U}$, and density fluctuation $\rho = \rho^* - \overline{\rho}$ ($\rho^*$: local absolute density, $\overline{\rho}$: background density) by the background density gradient $\mathcal{L}|\mathrm{d}\overline{\rho}/\mathrm{d}z|$. The vertical unit vector is $\mathbf{e}_z$. The non-dimensional parameters are

$$Fr_0 = \frac{\mathcal{U}}{N\mathcal{L}}\ , \quad Re_0 = \frac{\mathcal{U}\mathcal{L}}{\nu}\ , \quad Pr = \frac{\nu}{\mu} \tag{2}$$

We chose a Prandtl number of $Pr = 0.7$, corresponding to typical values in the atmosphere. Froude and Reynolds number are parameters that control the flow regime.

Without loss of generality, we assume that all mean velocity components are zero (Galilean invariance) and define the turbulence kinetic energy

$$E_k = \frac{1}{2}u_i u_i \tag{3}$$

and the available potential energy

$$E_p = \frac{1}{2}\rho^2/Fr_0^2. \tag{4}$$

The transport equations for the turbulence kinetic and the potential energy read

$$\partial_t E_k + \underbrace{\nabla \cdot (\mathbf{u}E_k)}_{-\mathcal{T}} = \underbrace{-\mathbf{u}\cdot\nabla p}_{\mathcal{P}} \underbrace{- \frac{\rho}{Fr_0^2}\mathbf{u}\cdot\mathbf{e}_z}_{\mathcal{B}} + \underbrace{\frac{1}{Re_0}\left[\nabla^2 E_k + (\nabla \mathbf{u})^2\right]}_{\mathcal{D}} + \underbrace{\mathbf{F}}_{\mathcal{F}} \tag{5a}$$

$$\partial_t E_p + \underbrace{\nabla \cdot \left(\mathbf{u}E_p\right)}_{-\mathcal{T}} = \underbrace{\frac{\rho}{Fr_0^2}\mathbf{u}\cdot\mathbf{e}_z}_{\mathcal{B}} + \underbrace{\frac{1}{Pr\ Re_0}\left[\nabla^2 E_p + \frac{(\nabla\rho)^2}{Fr_0^2}\right]}_{\mathcal{D}} \tag{5b}$$

where the single terms represent turbulent diffusion $\mathcal{T}$ (advection by turbulent velocity), pressure transport $\mathcal{P}$, buoyancy transport $\mathcal{B}$, molecular dissipation and diffusion $\mathcal{D}$, and external forces $\mathcal{F}$.

Our results will be presented in spectral space. The spectral kinetic energy density is defined as

$$\widehat{E_k} = \frac{1}{2}\widehat{u_i}\widehat{u_i}^*, \tag{6}$$

where $\widehat{u_i}$ are the Fourier-transformed velocity components and the asterisk $(\cdot)^*$ denotes the complex conjugate. The temporal rate of change of kinetic energy in spectral space is computed from

$$\widehat{\partial_t E_k} = \frac{1}{2}\left(\widehat{u_i}\widehat{\partial_t u_i}^* + \widehat{u_i}^*\widehat{\partial_t u_i}\right) = \widehat{\mathcal{T}}(E_k) + \widehat{\mathcal{P}}(E_k) + \widehat{\mathcal{B}}(E_k) + \widehat{\mathcal{D}}(E_k) + \widehat{\mathcal{F}}(E_k) \tag{7}$$

For evaluating the terms $\widehat{\mathcal{T}}$, $\widehat{\mathcal{P}}$, $\widehat{\mathcal{B}}$, $\widehat{\mathcal{D}}$, and $\widehat{\mathcal{F}}$, we use the respective term of the discretized transport equation to replace $\widehat{\partial_t u_i}$. The spectral buoyancy transport of kinetic energy, for example, is computed from

$$\widehat{\mathcal{B}}(E_k) = -\frac{\mathbf{e}_z}{2Fr_0^2}\cdot\left(\widehat{\mathbf{u}}\widehat{\rho}^* + \widehat{\mathbf{u}}^*\widehat{\rho}\right). \tag{8}$$

The spectral distribution of potential energy and its temporal derivative are defined accordingly.

With the spatial mean values of kinetic energy $\langle E_k \rangle$ and kinetic energy dissipation $\varepsilon_k = \langle \mathcal{D}(E_k) \rangle$, we define the integral flow scales

$$U_{\text{int}} = \langle E_k \rangle^{1/2} , \quad L_{\text{int}} = \frac{\langle E_k \rangle^{3/2}}{\varepsilon_k} \tag{9}$$

to find the local Froude and Reynolds number as well as the buoyancy Reynolds number $\mathcal{R}$, defined by Brethouwer et al. [5]:

$$Fr = \frac{Fr_0 \mathcal{L}}{\mathcal{U}} \frac{\varepsilon_k}{\langle E_k \rangle} , \quad Re = \frac{Re_0}{\mathcal{U}\mathcal{L}} \frac{\langle E_k \rangle^2}{\varepsilon_k} , \quad \mathcal{R} = Re\, Fr^2 = Re_0\, Fr_0^2\, \varepsilon_k \frac{\mathcal{L}}{\mathcal{U}^3} \tag{10}$$

In LES by construction, we do not have direct access to the values of $\varepsilon_k$ and $\varepsilon_p = \langle \mathcal{D}(E_p) \rangle$, as they are unresolved small-scale quantities. For LES, we thus estimate $\varepsilon_k$ from the total energy balance

$$\partial_t \langle E_t \rangle = \partial_t \langle E_k \rangle + \partial_t \langle E_p \rangle = P - \varepsilon_k - \varepsilon_p = P - (1 + \Gamma)\varepsilon_k, \tag{11}$$

where the temporal change of total energy in the flow $\langle E_t \rangle$ can be computed from the energy levels at subsequent time steps, $P$ is the power inserted into the system by the external forcing and $\Gamma = \varepsilon_p / \varepsilon_k$ is the mixing ratio assumed to be constant $\Gamma = 0.4$, which is an acceptable approximation for a wide range of parameters (cp. our DNS results, Fig. 2).

## 3 Numerical method

### 3.1 The adaptive local deconvolution method

Our approach to ILES is based on a nonlinear finite volume scheme involving a solution adaptive reconstruction (deconvolution) of the numerical solution. The nonlinear discretization scheme generates a certain controllable spectral numerical viscosity. Using an evolutionary optimization algorithm, free parameters of the discretization scheme have been calibrated in such a way that the effective spectral numerical viscosity is identical to the spectral eddy viscosity from turbulence theory for asymptotic cases [19]. In the following, we give a concise description of ALDM on the example of a one-dimensional generic transport equation

$$\partial_t u + \partial_x F(u) = 0. \tag{12}$$

For a more detailed description and the extension to the three-dimensional Navier-Stokes equations, we refer to Hickel et al. [19].

We obtain the discretized form of Eq. 12 by a convolution with a homogeneous filter kernel $G$ and a subsequent discretization of the filtered equations

$$\partial_t \overline{u}_N + G * \partial_x F_N(u_N) = -G * \partial_x \cdot \tau_{\text{sgs}} = \mathcal{G}_{\text{sgs}}, \tag{13}$$

where the overbar indicates spatial filtering and the subscript $N$ denotes the discretized solution on a numerical grid. In Eq. 13 we use the unfiltered solution to compute the nonlinear term, which requires the deconvolution of the solution on the range of represented scales $u_N = G^{-1} * \overline{u}_N$.

The truncation error of a numerical reconstruction scheme can be written as

$$\mathcal{G}_{\text{num}} = G * \partial_x F_N(u_N) - \tilde{G} * \tilde{\partial}_x \tilde{F}_N(\tilde{u}_N), \tag{14}$$

where the tilde indicates discrete numerical approximations. While the exact continuous solution $u$ is unknown, we can obtain the numerical approximation $\tilde{u}_N$ of the grid function $u_N$ by a regularized deconvolution of $\overline{u}_N$ [10]. The discrete filtered solution of our numerical method then satisfies the modified differential equation

$$\partial_t \overline{u}_N + G * \partial_x F_N(u_N) = \mathcal{G}_{\text{num}} + \tilde{\mathcal{G}}_{\text{sgs}}, \tag{15}$$

which is identical to Eq. 13 if $\mathcal{G}_{\text{num}} + \tilde{\mathcal{G}}_{\text{sgs}} = \mathcal{G}_{\text{sgs}}$. Explicit SGS modeling is based on the assumption $\mathcal{G}_{\text{num}} = 0$. In implicit LES, the numerical error acts as an implicit SGS model: $\mathcal{G}_{\text{num}} = \mathcal{G}_{\text{sgs}}$ and no explicit SGS model is used, i.e., $\tilde{\mathcal{G}}_{\text{sgs}} = 0$. The transport equation eventually to be solved is

$$\partial_t \overline{u}_N + \tilde{G} * \tilde{\partial}_x \tilde{F}_N(\tilde{u}_N) = 0, \tag{16}$$

where no model terms are computed explicitly.

Finite volume methods such as ALDM require a local approximation of the unfiltered solution at the cell faces (indicated by half-integer indices), which we find by a nonlinear combination

$$\tilde{u}_N^{\mp}(x_{j\pm1/2}) = \sum_{k=1}^{K}\sum_{r=0}^{k-1} \omega_{k,r}^{\mp}(\overline{u}_N)\,\tilde{p}_{k,r}^{\mp}(x_{j\pm1/2}) \tag{17}$$

of Harten-type polynomials [15]

$$\tilde{p}_{k,r}^{\mp}(x_{j\pm1/2}) = \sum_{l=0}^{k-1} c_{k,r,l}^{\mp}(x_N)\,\overline{u}_{j-r+l}. \tag{18}$$

The deconvolution is solution adaptive by weighting the contributions of the different polynomials by the coefficients $\omega_{k,r}^{\mp}(\overline{u}_N)$, which represent the smoothness of the solution $\overline{u}_N$, see [19]. The grid-dependent coefficients $c_{k,r,l}^{\mp}(x_N)$ are chosen such that the polynomial $\tilde{p}_{k,r}^{\mp}(j \pm 1/2)$ is a $k$-th order approximation of the unfiltered solution. The reconstructed solution $\tilde{u}_N^{\mp}$ is used in a consistent numerical flux function

$$\tilde{F}_N(x_{j\pm1/2}) = F\left(\frac{\tilde{u}_{j\pm1/2}^{-} + \tilde{u}_{j\pm1/2}^{+}}{2}\right) - \sigma_{j\pm1/2}\left(\tilde{u}_{j\pm1/2}^{+} - \tilde{u}_{j\pm1/2}^{-}\right). \tag{19}$$

Both the reconstruction scheme and the flux function introduce free parameters, which can be used to control the truncation error. Our objective is not a maximum order of accuracy but a physically correct representation of the effects of unresolved turbulence. For this purpose, Hickel et al. [19] performed a spectral space analysis of the effective viscosity of ALDM. They optimized the free parameters such that the spectral numerical viscosity of ALDM matches the spectral eddy viscosity from the eddy-damped quasi-normal Markovian (EDQNM) theory for isotropic turbulence. This single set of parameters has not been changed since it was once settled and is also used for the computations we are presenting here. Although optimized for the asymptotic case of isotropic turbulence, ALDM has proven to yield good results for a large variety of complex turbulent flows. This includes decaying turbulence [19], boundary layer flows [17,18], separated flows [21], and others. ALDM yields good results also for cases of anisotropic and inhomogeneous turbulence.

Hickel et al. [20] extended ALDM to the transport of passive scalars. This basically employs the same framework, but a distinction is made between two different regimes depending on the Schmidt number. For high Schmidt numbers $\mathrm{Sc} \gg 1$, the passive scalar spectrum has two distinct inertial ranges, which is taken into account by using a different set of optimized model parameters. For the case $\mathrm{Sc} \lesssim 1$, which applies to the present simulations, the spectra of turbulence kinetic and potential energy are similar and thus the same set of parameters can be used for momentum and scalar transport equations. We adopted this implicit SGS model for passive scalar transport for the active scalar equation. This is possible since the feedback from the density field onto the velocity field does not originate from a nonlinear term but from the linear buoyancy term.

In the original formulation, Hickel et al. [20] used the reconstructed velocity field $\tilde{u}$ to compute the numerical flux function for the scalar transport. Since the reconstructed velocity $\tilde{u}$ is in general not divergence-free, an additional divergence correction term is necessary to avoid the generation of artificial fluctuations in a uniform scalar field. In the present implementation, we avoid this difficulty by using the filtered (defined on a staggered Cartesian mesh and therefore divergence-free) velocity field $\overline{u}_N$ for the transport velocity in the scalar flux. The numerical flux function in the scalar transport equation then reads

$$\tilde{F}_{j\pm1/2}^{s} = \overline{u}_{j-1/2\pm1/2}\frac{\tilde{c}_{j\pm1/2}^{-} + \tilde{c}_{j\pm1/2}^{+}}{2} - \sigma_C\left|\tilde{u}_{j\pm1/2}^{-} - \tilde{u}_{j-1\pm1/2}^{+}\right|\left(\tilde{c}_{j\pm1/2}^{+} - \tilde{c}_{j\pm1/2}^{-}\right). \tag{20}$$

This modified numerical flux function has been tested against the original implementation for neutrally and stably stratified turbulence. As there was no recognizable effect on the flow energy spectra, we used the simplified formulation throughout the present study.

### 3.2 Computational details

With our flow solver INCA, the Boussinesq equations are discretized by a fractional step method on a staggered Cartesian mesh. The code is parallelized both for shared and distributed memory systems and it offers different discretization schemes depending on the application. For time advancement, the explicit third-order Runge-Kutta scheme of Shu [32] is used. The time step is dynamically adapted to satisfy a Courant-Friedrichs-Lewy condition with CFL = 1.0. The spatial discretization is a finite volume method. For DNS and LES with explicit SGS model, we use a non-dissipative central difference scheme with fourth-order accuracy for the convective terms and second-order central differences for the diffusive terms and the pressure Poisson solver. For implicit LES, the central difference scheme for the convective terms is replaced by the implicit turbulence model ALDM. The Poisson equation for the pressure is solved at every Runge-Kutta substep. The Poisson solver employs fast Fourier-transform in the vertical direction and a Stabilized Bi-Conjugate Gradient (BiCG-STAB) solver [37] in the horizontal plane. By the FFT, the three-dimensional problem is transformed into a set of independent two-dimensional problems, which can be solved in parallel. All computations presented here were run on Cartesian grid blocks with uniform cell size.

### 3.3 Numerical set-up of homogeneous stratified turbulence

We simulate homogeneous turbulence with stable stratification in a triply-periodic box. The turbulence kinetic energy is maintained at an approximately constant level by a volume force at small wavenumbers. As proposed in [5,16,28,38], the forcing is only applied to horizontal wavenumbers of the horizontal velocity components. The time- and space-dependent forcing term reads [1]

$$\mathbf{F}(\mathbf{x}, t) = \sum_{k_i, k_j = 1}^{2} \mathbf{a}_{i,j} \cos(2\pi k_i x + p_{i,j}) \cos(2\pi k_j y + q_{i,j}). \tag{21}$$

The random amplitudes $\mathbf{a}_{i,j}$ and phases $p_{i,j}$ and $q_{i,j}$ are recomputed at every time step so that no mean velocity is forced in any direction. Additionally, the forcing term is scaled with a spatially constant factor in such a way that the forcing power achieves a prescribed value. Thus, the amount of input energy per time unit is kept constant and variations of the total flow energy are only due to variations in the dissipation rate. The forcing is applied at wavenumbers $k_i, k_j \in [1, 2]$, which corresponds to lengthscales $L_f \in [0.5\mathcal{L}, \mathcal{L}]$, where $\mathcal{L} = 2\pi$ is an arbitrary length scale. In the statistically steady state, the mean dissipation rate becomes equal to the forcing power. Hence we can control the total energy dissipation rate by fixing the forcing power. We choose the forcing power to be $P = 1/(2\pi)$ and a unity velocity scale $\mathcal{U}$. Thus, the integral turbulence length scale $L_{\mathrm{int}} = \mathcal{U}^3/\varepsilon$ is of the same order as $\mathcal{L}$.

The computations are initialized with low-level white noise. Due to the constant energy injection by the forcing, the flow energy increases linearly in time. Vertical vortices gain intensity until they break down due to the inherent instability of the flow [2]. This transition was completed in all computations after 30–40 time units. We usually computed the transition phase on a coarse grid. Then, we interpolated the results to the final fine grid and continued the computation on the fine grid. An example time series of energy and dissipation rate is displayed in Fig. 1.

We present the result of three series of direct numerical simulations. A detailed list with the parameters of the computations is given in Table 1. The series differ in their Reynolds number, which is approximately 5,000 for series A, 10,000 for series B, and 25,000 for series C. Within each series we chose a set of different Froude numbers between 0.01 and 0.2 and simulated also a neutrally stratified case, which corresponds to an infinite Froude number. To reduce the number of grid points, the domain size in the vertical direction is reduced by 50% the cases with $\mathcal{R} < 50$, except for the third series. This was possible since the vertical length scales are expected to be much smaller than the horizontal ones if the stratification has a considerable influence.

The LES were performed with the same set of parameters and domain size as the DNS. The LES resolution is $64^3$ grid cells, unless stated otherwise.

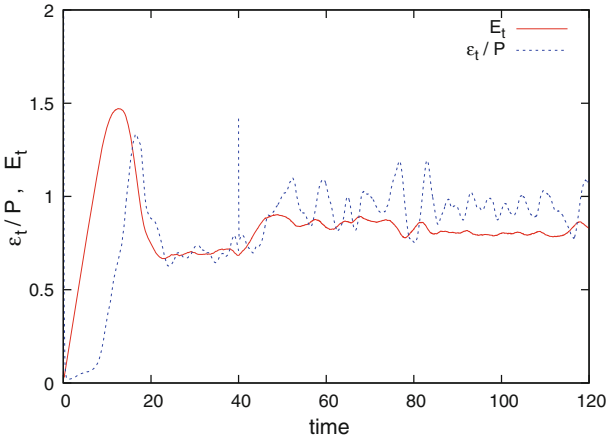


**Fig. 1** Total energy and dissipation rate over time for a single DNS. At $t = 40$ we switched from the coarse to the fine grid, which generates a peak in the dissipation rate

**Table 1** List of direct numerical simulations of forced stratified turbulence

| # | $Re$ | $Fr$ | $\mathcal{R}$ | $N_h$ | $N_v$ | $L_v/\pi$ | $\eta k_{\max}$ |
|---|---|---|---|---|---|---|---|
| A1 | 3,700 | 0.017 | 1.1 | 320 | 160 | 1 | 2.3 |
| A2 | 3,700 | 0.028 | 2.8 | 320 | 160 | 1 | 2.3 |
| A3 | 4,900 | 0.033 | 5.3 | 320 | 160 | 1 | 1.9 |
| A4 | 5,300 | 0.044 | 10.4 | 320 | 160 | 1 | 1.8 |
| A5 | 4,200 | 0.099 | 41.3 | 320 | 160 | 1 | 2.1 |
| A6 | 4,900 | 0.162 | 126.7 | 320 | 320 | 2 | 1.9 |
| A7 | 4,800 | 0.304 | 448.1 | 320 | 320 | 2 | 1.9 |
| B1 | 7,100 | 0.017 | 2.1 | 640 | 320 | 1 | 2.8 |
| B2 | 6,100 | 0.025 | 3.7 | 640 | 320 | 1 | 3.2 |
| B3 | 8,300 | 0.027 | 6.3 | 640 | 320 | 1 | 2.6 |
| B4 | 11,800 | 0.035 | 14.2 | 640 | 320 | 1 | 2.0 |
| B5 | 9,300 | 0.067 | 41.4 | 640 | 640 | 2 | 2.4 |
| B6 | 9,600 | 0.201 | 387.6 | 640 | 640 | 2 | 2.2 |
| B7 | 8,400 | $\infty$ | $\infty$ | 480 | 480 | 2 | 1.7 |
| C1 | 23,000 | 0.010 | 2.4 | 960 | 960 | 2 | 2.8 |
| C2 | 22,700 | 0.020 | 9.5 | 960 | 960 | 2 | 3.2 |
| C3 | 28,900 | 0.034 | 33.7 | 960 | 960 | 2 | 2.6 |

Within the series A, B, and C, the simulations have roughly the same Reynolds number. $N_h$ and $N_v$ are the number of cells in horizontal and vertical direction, respectively. $L_v$ is the vertical domain size. The horizontal domain size was $L_h = 2\pi$ in all cases. The product of Kolmogorov length $\eta$ and the maximum resolved wavenumber $k_{\max}$ is an indicator of the resolution of the smallest turbulent scales. It should be larger than one for any DNS

## 4 Results

### 4.1 Direct numerical simulations

#### *4.1.1 Integral flow data*

In Fig. 2, we show the mixing efficiency $\varepsilon_p/\varepsilon_k$ as well as the ratio of potential to kinetic energy $E_p/E_k$ as functions of the buoyancy Reynolds number. These plots include the results from all three series of DNS. Additionally, we added the results from Brethouwer et al. [5]. For low $\mathcal{R}$, the mixing efficiency increases with increasing $\mathcal{R}$. This confirms the results of Brethouwer et al. [5]. In the region with $\mathcal{R} \gtrsim 100$, we find a decreasing mixing efficiency. The computations in the high $\mathcal{R}$ region all have a comparatively high Froude number (larger than 0.1), which means that they are only weakly affected by stratification effects and thus do not necessarily follow the same scaling as the stronger stratified cases. Thus, we cannot conclude with certainty whether the decreasing mixing efficiency is an effect of Froude or buoyancy Reynolds number. The peak value of $\varepsilon_p/\varepsilon_k$ is between 0.4 and 0.5, which agrees with common assumptions.

The ratio of potential to kinetic energy $E_p/E_k$ is not a universal quantity as the mixing efficiency since it is directly influenced by the forcing, but still we can find a certain trend depending on the buoyancy Reynolds

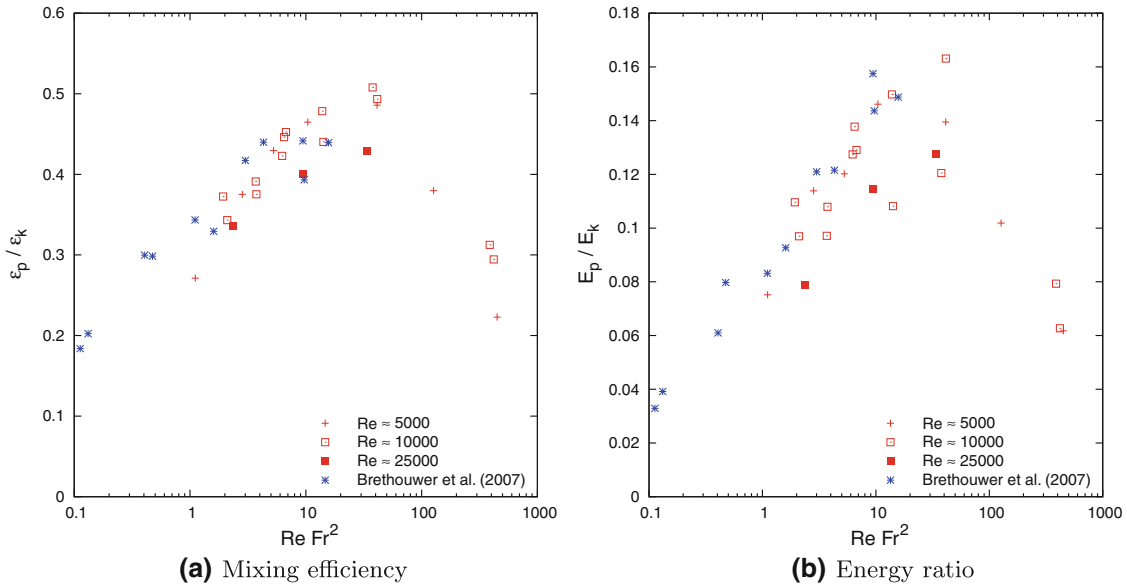


**(a)** Mixing efficiency **(b)** Energy ratio

**Fig. 2** Integral ratios of kinetic to potential energy and dissipation rates in stratified turbulence (DNS)

number. Similarly to the mixing efficiency, it has a peak in the region $10 < \mathcal{R} < 100$, although the results scatter a bit more than for the mixing efficiency. This shows that large-scale features (energy ratio) and small-scale features (mixing efficiency) evolve in a similar manner if the stratification is gradually increased.

### *4.1.2 Effects of stratification*

The energy spectrum of homogeneous turbulence is a function of the three-dimensional wavenumber space. If we assume that the flow is isotropic in the horizontal plane, we can reduce this to a two-dimensional representation. We removed the second horizontal direction by averaging the spectrum on circles with constant distance from the vertical axis ($k_h$) and constant vertical wavenumber ($k_v$).

To illustrate the influence of stable stratification on the energy spectra, we show in Figs. 3, 4, 5, 6 results from the second series of DNS with Reynolds numbers of approximately 10,000. The three cases chosen include a strongly stratified case ($Fr = 0.017$, $\mathcal{R} = 2.1$), a moderately stratified case ($Fr = 0.035$, $\mathcal{R} = 14.2$), and a neutrally stratified case ($Fr = \infty$) for comparison.

The energy spectra of the three selected cases are presented in Fig. 3. In the neutral case, the horizontal kinetic energy is distributed quite isotropically, if we ignore the local influence of the large-scale horizontal forcing. For increasing stratification, the vertical modes of $E_h$ contain increasingly more energy than the horizontal modes of the same absolute wavenumber. This corresponds to integral flow structures that have large horizontal and small vertical scales. Note that the peak energy density for the strongly stratified example is more than one order of magnitude higher than in the neutral case, while the integral amount of energy is similar in both cases.

The effect of stratification on the vertical kinetic energy is remarkably different. We find that the distribution of $E_v$ is less anisotropic than $E_h$, especially for the strongly stratified case. Here, the peak energy density decreases, since the integral amount of vertical kinetic energy decreases for strong stratification. The potential energy spectrum has features of both kinetic energy spectra. It shows an agglomeration of energy near the vertical axis, just like the horizontal kinetic energy spectrum, but on the other hand, there is also a significant contribution on horizontal modes for medium wavenumbers.

To help understanding the mechanisms that lead to the mean energy spectra presented before, we analyze the spectra of the different terms in the transport equation of turbulence energy. To account for the fact that regions with large horizontal wavenumbers contribute more to the total change of energy than region close to the vertical axis, we show here spectra *integrated* over circles with constant horizontal and vertical wavenumber rather than averaged spectra.

We show the spectra of turbulent diffusion in Fig. 4. Horizontal kinetic energy is transported away from the region of forcing (which is not displayed in the double-logarithmic plot, since it has a zero vertical wavenumber)

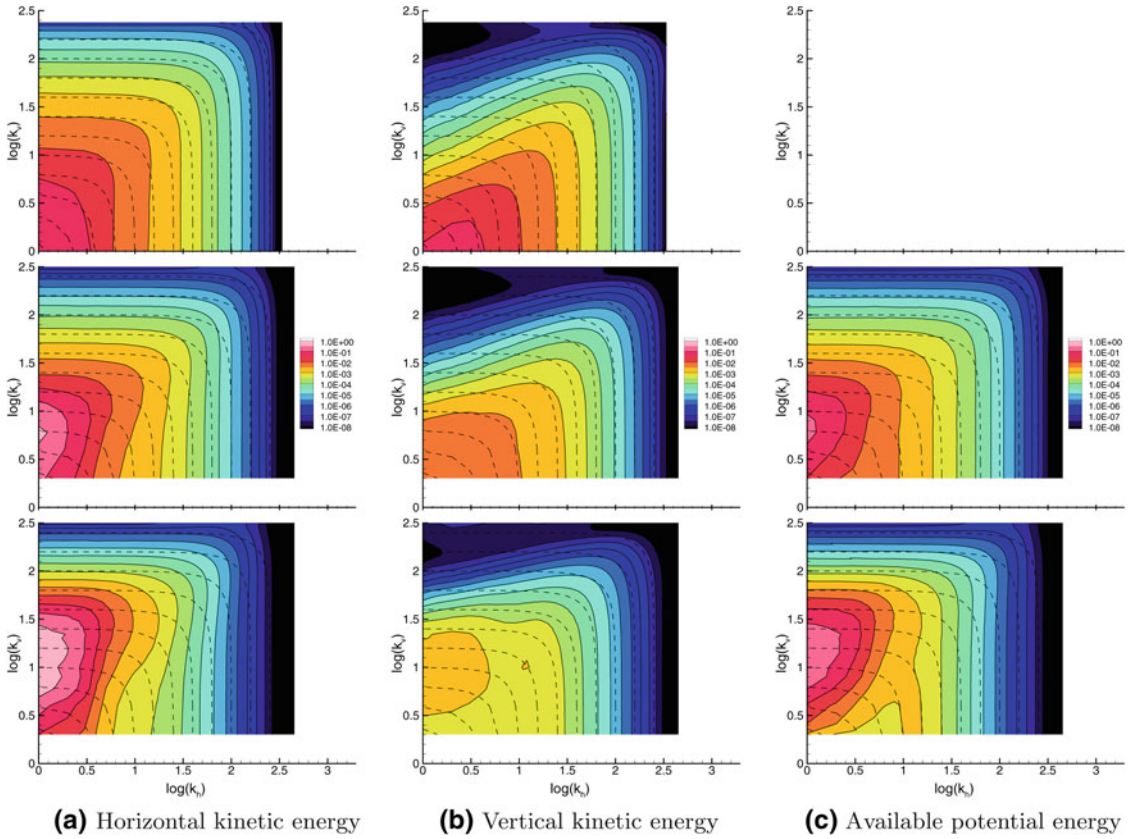


**Fig. 3** Two-dimensional energy spectra of homogeneous stratified turbulence with $Re \approx 10{,}000$ (Simulations B1, B4, and B7). *Solid lines*: energy contours (adjacent contour lines are separated by a factor of $\sqrt{10}$), *dashed lines*: iso-lines of total wavenumber $\sqrt{k_h^2 + k_v^2}$. *First row*: neutral stratification ($Fr = \infty$), *second row*: weak stratification ($Fr = 0.035$), *third row*: strong stratification ($Fr = 0.017$)

to smaller scales. For vertical kinetic energy, we find a transport from large to small scales only in the neutrally stratified case. As soon as stable stratification comes into play, it is more a transport away from vertical or diagonal[1] modes to horizontal modes. This explains the isotropic distribution of $E_v$, we have seen in the preceding section.

The molecular diffusion and dissipation spectra in Fig. 5 show that for strong stratification the activity of molecular dissipation of horizontal kinetic energy and potential energy is concentrated in the vertical modes, where the peak values of the respective energy spectra are located. This does not apply to the vertical kinetic energy, which is dissipated more or less isotropically at small scales.

The gap between turbulent diffusion and molecular dissipation is closed by the pressure term, Fig. 6a, which basically converts horizontal kinetic energy into vertical kinetic energy and the buoyancy term, Fig. 6b, which converts vertical kinetic energy into available potential energy. Both terms act on similar medium scales.

We can summarize the evolution of energy in strongly stratified turbulence as follows: Horizontal turbulence kinetic energy $E_h$, being produced by a forcing on large horizontal scales, is transported to medium vertical and diagonal scales by turbulent diffusion (advection by the turbulent velocity field). A certain fraction, especially in the vertical modes, is directly dissipated by molecular viscosity, the rest is turned into vertical kinetic energy $E_v$ by the pressure term. Turbulent diffusion equilibrates the distribution of $E_v$ by transferring part of it to medium horizontal modes. A small amount of $E_v$ is dissipated, the rest is converted into available potential energy $E_p$ by buoyancy. $E_p$ is transferred to small vertical scales by turbulent diffusion, where it is eventually extracted from the system by molecular dissipation.

[1] As diagonal modes we refer to the region where vertical and horizontal wavenumber are similar. This corresponds to isotropically shaped structures in real space.

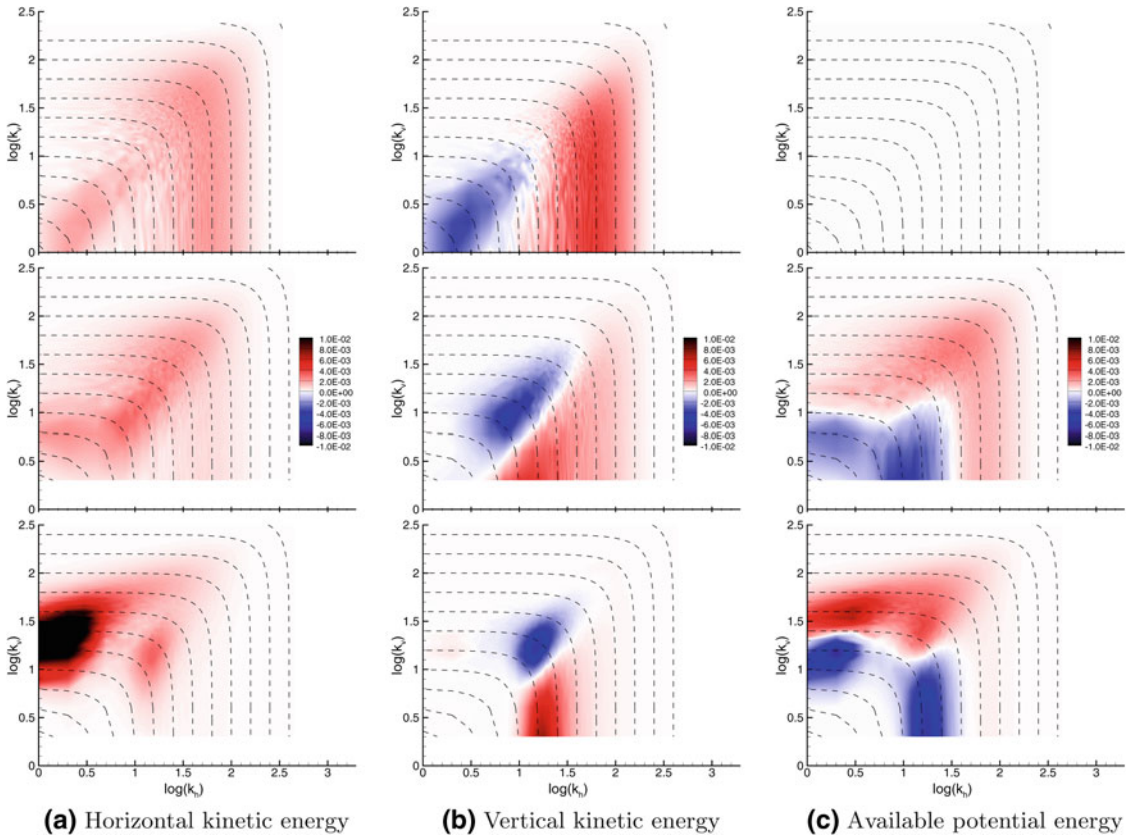


**Fig. 4** Two-dimensional spectra of turbulent diffusion $\widehat{\mathcal{T}}$ in homogeneous stratified turbulence with $Re \approx 10{,}000$. *Dashed lines* indicate constant total wavenumber. $Fr = \infty, 0.035, 0.017$ (cf. Fig. 3)

### *4.1.3 Reynolds number effects*

In the preceding section, we have discussed the effects of varying Froude number on the energy spectra. The second important issue is the influence of the Reynolds number. Certainly, increasing the Reynolds number will shift the dissipation range to smaller scales and increase the size of the inertial range. According to Brethouwer et al. [5], the spectra are self-similar at constant buoyancy Reynolds number. On the other hand, the anisotropy of turbulence is governed by the Froude number. The question is then how the spectra change if the Reynolds number is changed and the Froude number or buoyancy Reynolds number, respectively, are held constant.

In Fig. 7, we show the spectra of horizontal kinetic energy for cases with different Reynolds numbers. In the top row, the buoyancy Reynolds number is approximately held constant, while the Froude number is changed. In the bottom row, the Froude number is approximately constant. Generally, the dissipative range of the spectrum is shifted to higher wavenumbers as the Reynolds number increases, since the Kolmogorov length scale decreases. So the small-scale range of the spectra does not show any unexpected behavior. The energy containing region, however, looks different in the scenario with $\mathcal{R} \approx$ const compared to a constant Froude number. Only for the latter variation we find a similar peak region for all three Reynolds numbers. For constant buoyancy Reynolds number, on the other hand, the peak is shifted to larger vertical wavenumbers as the Reynolds number is increased (which means a decreased Froude number).

This observation is confirmed by studying the energy transfer spectra. As an example, we show the buoyancy transport spectrum of vertical kinetic energy in Fig. 8. For $\mathcal{R} \approx$ const we observe a shift of the main activity of the buoyancy term to smaller scales at higher Reynolds number. Especially, the separation of the activity into two distinct regions, one on vertical modes and one more on horizontal modes, only arises if the Froude number is sufficiently low. On the other hand, for Fr $\approx$ const the distribution of buoyancy fluxes looks similar for all Reynolds numbers. Only the "tail" of the horizontal region reaches to smaller horizontal scales.

In summary, we find that the relevant parameter determining the shape of the spectrum in the strongly stratified regime is the Froude number. It controls the distribution of the most energetic modes in the spectrum

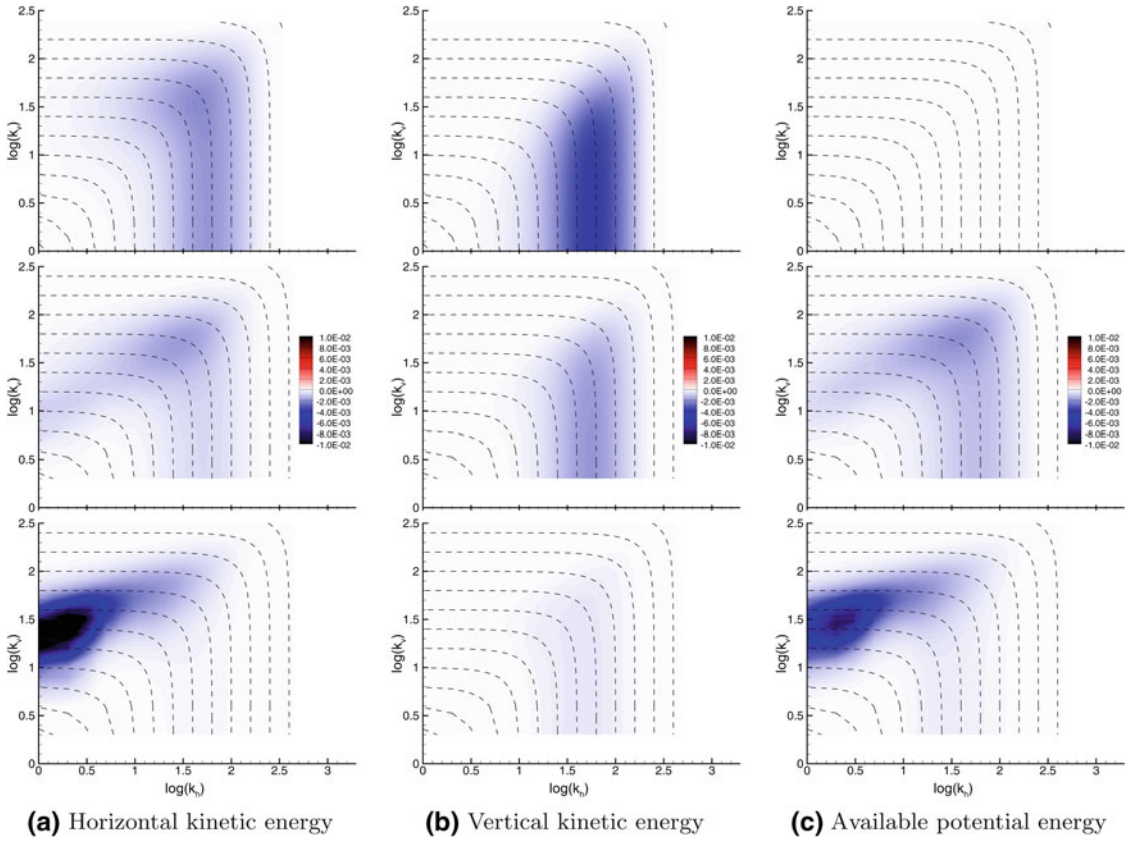


**Fig. 5** Two-dimensional spectra of molecular diffusion and dissipation $\widehat{\mathcal{D}}$. *Dashed lines* indicate constant total wavenumber. $Fr = \infty, 0.035, 0.017$ (cf. Fig. 3)

and the anisotropy of turbulence. The Reynolds number, in the other hand, just changes the range of scales of turbulence but does not influence the large scales. This is in good agreement to common knowledge about isotropic turbulence.

## 4.2 Large eddy simulations

### *4.2.1 Integral flow data*

The first criterion for the validation of an LES method is its ability to correctly reproduce the ratios of the different types of energy from the DNS. In Fig. 9a, we show again the ratio of potential to kinetic energy versus buoyancy Reynolds number. The results from a number of LES are included. They match very well with the DNS results for most of the parameter space. Just for the lowest buoyancy Reynolds number, the energy ratio is under-predicted by the LES. However, in this region the flow is not turbulent any more but in the transition to the "viscosity affected stratified" regime [5], which we presently do not want to address.

In Fig. 9b, we make the comparison for the ratio of vertical kinetic energy to potential energy. In our horizontally forced scenario, this ratio of energies is the only one which is not affected by the forcing. We thus can assume that it will follow a universal trend. $E_v/E_p$ monotonically decreases if the Froude number decreases. This emphasizes the growing influence of the buoyancy transport with increasing stratification. In the DNS, the rate of change of the energy ratio is approximately $Fr^{0.82}$. If plotted over the Froude number, the results from all DNS with different Reynolds number are within a comparably narrow band. On the other hand, in a plot as a function of buoyancy Reynolds number, one could see a significant influence of Reynolds number. We conclude that the Froude number is also the relevant parameter to control the ratio $E_v/E_p$.

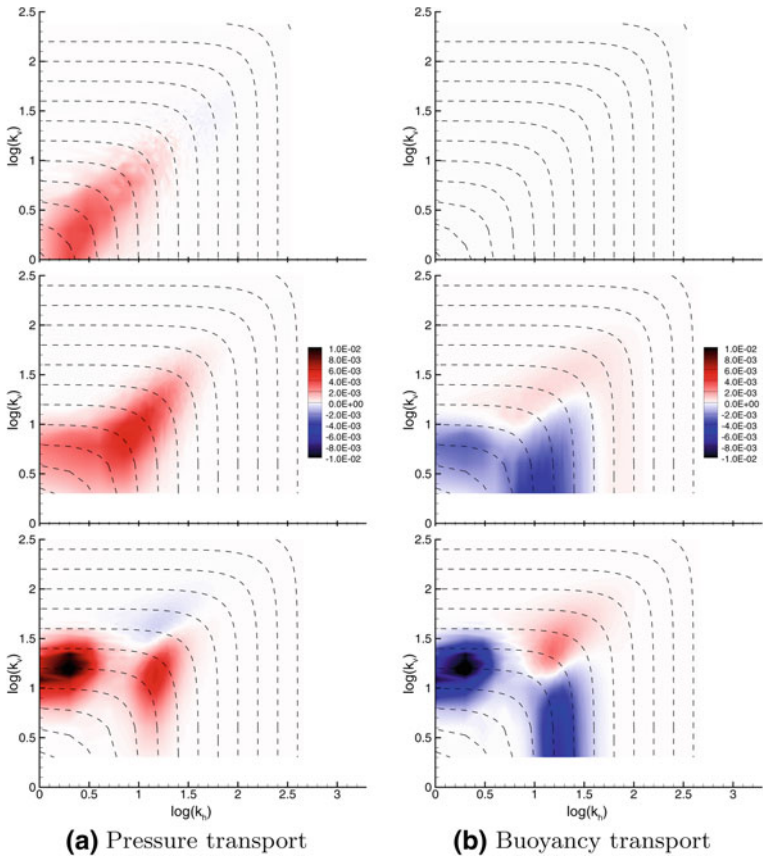


**Fig. 6** Two-dimensional spectra of pressure transport $\widehat{\mathcal{P}}$ and buoyancy transport $\widehat{\mathcal{B}}$ of vertical kinetic energy. *Dashed lines* indicate constant total wavenumber. $Fr = \infty, 0.035, 0.017$ (cf. Fig. 3)

With the implicit LES model ALDM, we find the same trend for the energy ratio. For large Froude numbers, the agreement with DNS is very good, whereas for stronger stratification ALDM systematically under-predicts $E_v/E_p$. The exponent for the rate of change is slightly higher, i.e., approximately 0.95. This result is, however, still in much better agreement with the DNS than the results obtained with the standard Smagorinsky model (SSM). For high Froude numbers, the SSM predicts the energy ratio with good accuracy, but for stronger stratified flows the decay of vertical kinetic energy compared to potential energy is strongly over-predicted. The large eddy simulations with ALDM and SSM, respectively, were computed on the same computational grids. Hence, the different result is due to the different ability of both SGS models to adapt to strongly anisotropic conditions. ALDM clearly shows a better performance in strongly stratified cases.

### *4.2.2 One-dimensional energy spectra*

For comparison of kinetic energy spectra, we selected one DNS in the weakly stratified regime ($\mathcal{R} = 41$, $Fr = 0.07$, $Re = 9{,}300$) in Fig. 10 and strongly stratified regime ($\mathcal{R} = 6.3$, $Fr = 0.03$, $Re = 8{,}300$) in Fig. 11. The corresponding LES have similar Froude and Reynolds numbers.

In the horizontal spectra of kinetic energy, the difference between ALDM and an explicit eddy viscosity model is most obvious. In the weakly stratified case ($\mathcal{R} = 41$), the horizontal spectrum is still quite similar to the Kolmogorov spectrum of isotropic turbulence. In this case, both SGS models predict the inertial range spectrum fairly well. The SSM is slightly too dissipative, but the difference from the DNS spectrum is acceptable. Things completely change for the stronger stratified case ($\mathcal{R} = 6.3$). The SSM dissipates too much energy and thus under-predicts the inertial range spectrum by more than one order of magnitude. Additionally, the predicted power-law exponent is significantly lower than $-5/3$. The spectrum predicted by ALDM, on the other hand, agrees well with the DNS. It correctly predicts the characteristic plateau region between the

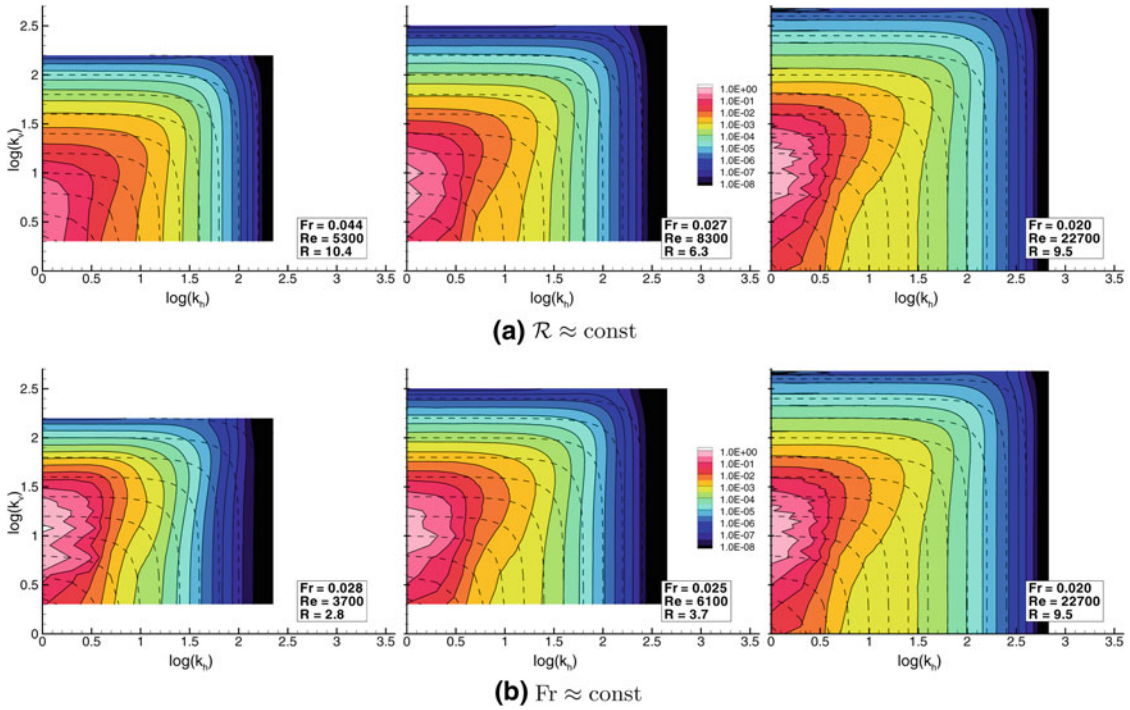


**Fig. 7** Two-dimensional spectra of horizontal kinetic energy for different Reynolds numbers. *Dashed lines* indicate constant total wavenumber. **a** Simulations A4, B3, and C2; **b** simulations A2, B2, and C2

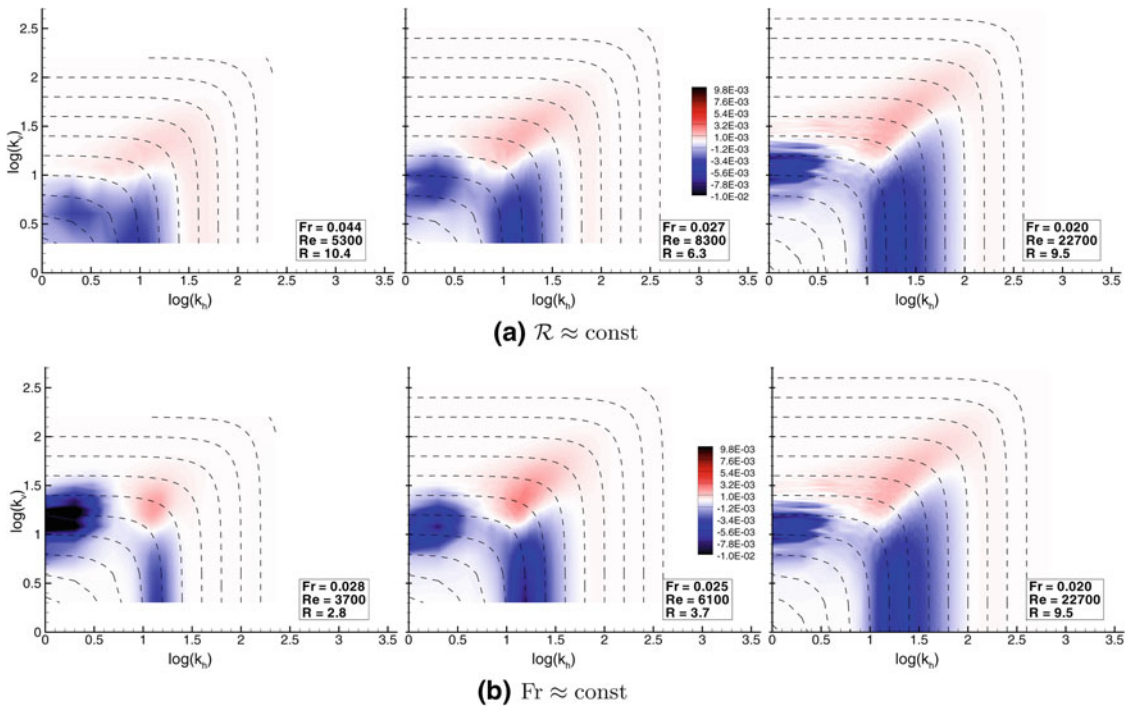


**Fig. 8** Two-dimensional spectra of buoyancy transport $\widehat{\mathcal{B}}$ of vertical kinetic energy for different Reynolds numbers. *Dashed lines* indicate constant total wavenumber

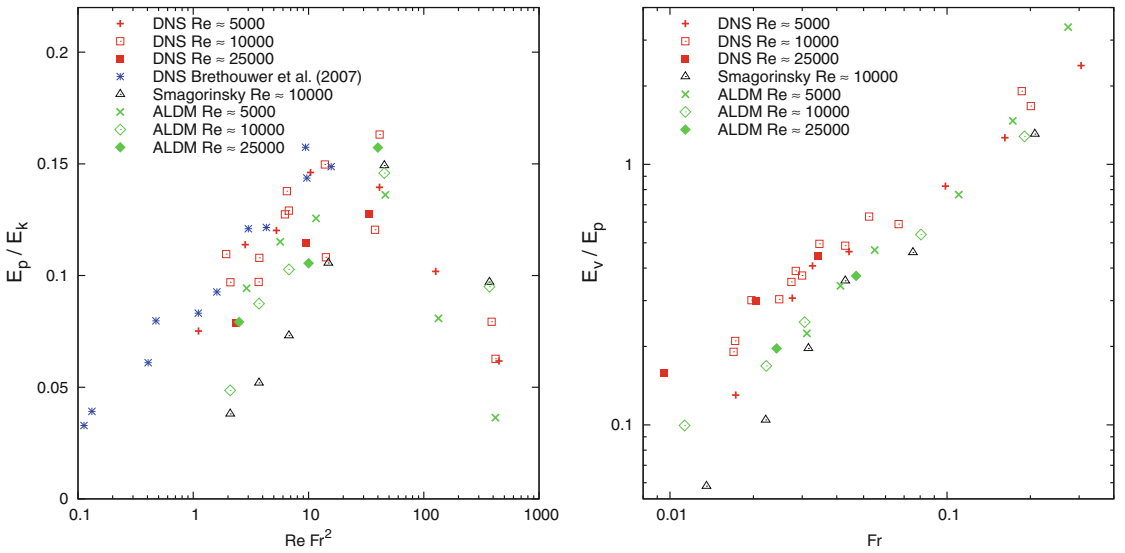


**(a)** Ratio of potential energy to kinetic energy **(b)** Ratio of vertical kinetic energy to potential energy

**Fig. 9** Integral energy ratios in stratified turbulence. Comparison of DNS and LES results

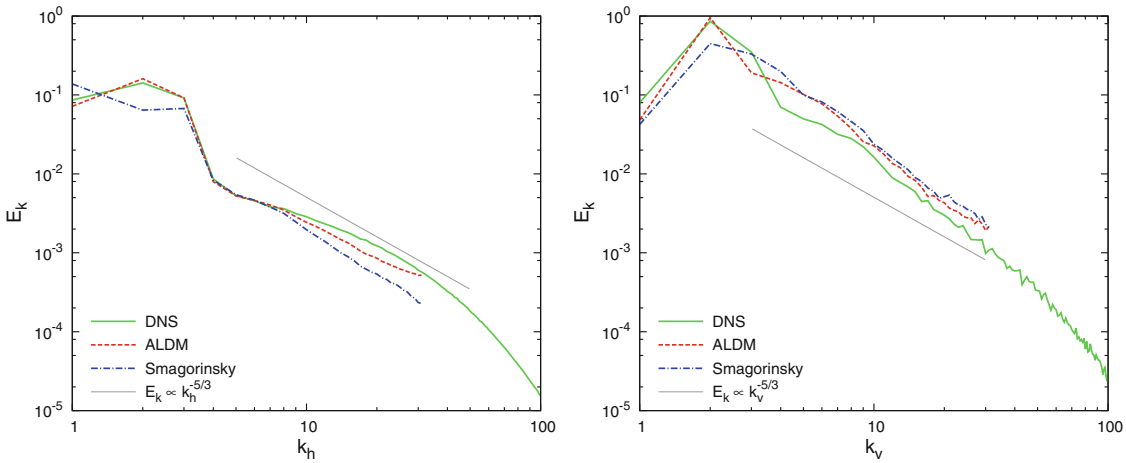


**(a)** Horizontal spectra **(b)** Vertical spectra

**Fig. 10** Weakly stratified turbulence kinetic energy spectra ($\mathcal{R} = 41$)

forcing scales and the inertial scales. Moreover, it produces a power-law decay with an exponent of $-5/3$, corresponding to the DNS[2] and theory derived from scaling laws [5].

In the vertical spectra of kinetic energy, the inertial range decay exponent changes from $-5/3$ in neutrally stratified fluid to $-3$ in strongly stratified turbulence. We find this change in the DNS and it is well reproduced by the LES. Both SGS models predict the turbulence inertial range decay well. At strong stratification, the ALDM result perfectly agrees with the DNS. The SSM result is slightly too dissipative in this region.

### *4.2.3 Two-dimensional energy spectra*

We compare the two-dimensional energy spectra of a strongly stratified case ($\mathcal{R} = 3.7$) in Fig. 12. In the DNS spectra, the LES domain is indicated by a black rectangle to simplify visual comparison with the LES results. The ILES spectra of all three types of energy compare well the corresponding DNS spectra, although the ILES

[2] In fact, the inertial range is not clearly visible in the DNS due to the low buoyancy Reynolds number $\mathcal{R}$. Similar spectra were, for example, reported by Brethouwer et al. [5].

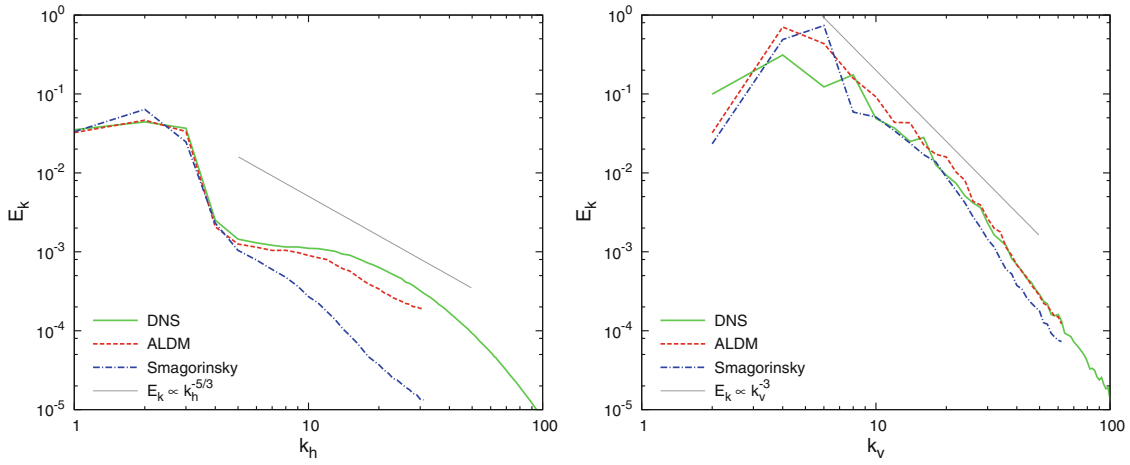


**(a)** Horizontal spectra **(b)** Vertical spectra

**Fig. 11** Strongly stratified turbulence kinetic energy spectra ($\mathcal{R} = 6.3$)

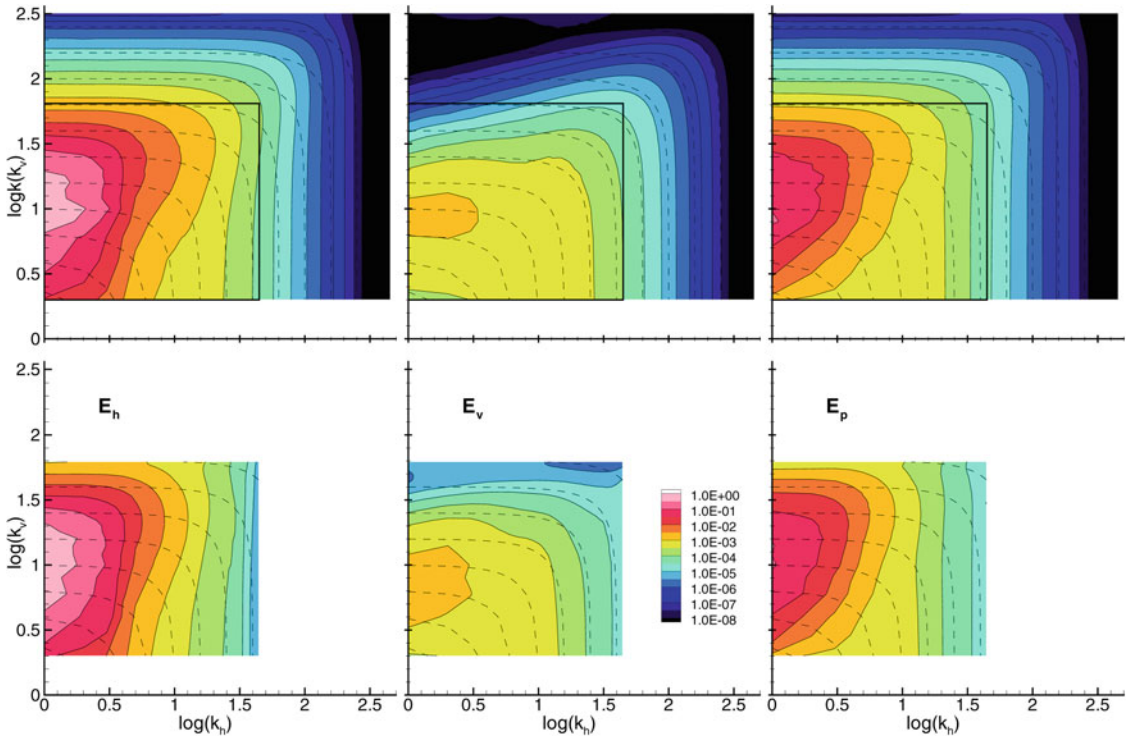


**Fig. 12** Two-dimensional energy spectra of stratified turbulence ($Fr = 0.025$, $Re = 6{,}100$, $\mathcal{R} = 3.7$). DNS (*top row*) and ILES with ALDM (*bottom row*)

was computed on a coarse grid of only $64^3$ cells, while the DNS needed $640^2 \times 320$ cells. The ILES resemble the large-scale features of the DNS very well and also correctly predict the vertical spectrum up to the cut-off wavenumber. At high horizontal wavenumbers, we observe a slight under-prediction of the energy levels, as we have already seen in the one-dimensional spectra (Figs. 10 and 11).

The ILES are also capable of accurately predicting the spectra of turbulent diffusion (Fig. 13). At high horizontal wavenumbers, the computed values of $\widehat{\mathcal{T}}$ are smaller in the ILES solution compared to the corresponding DNS results. This discrepancy is due to the lower energy level observed there. However, the anisotropic shape of the two-dimensional spectra and the relative intensities of energy are predicted in an excellent way.

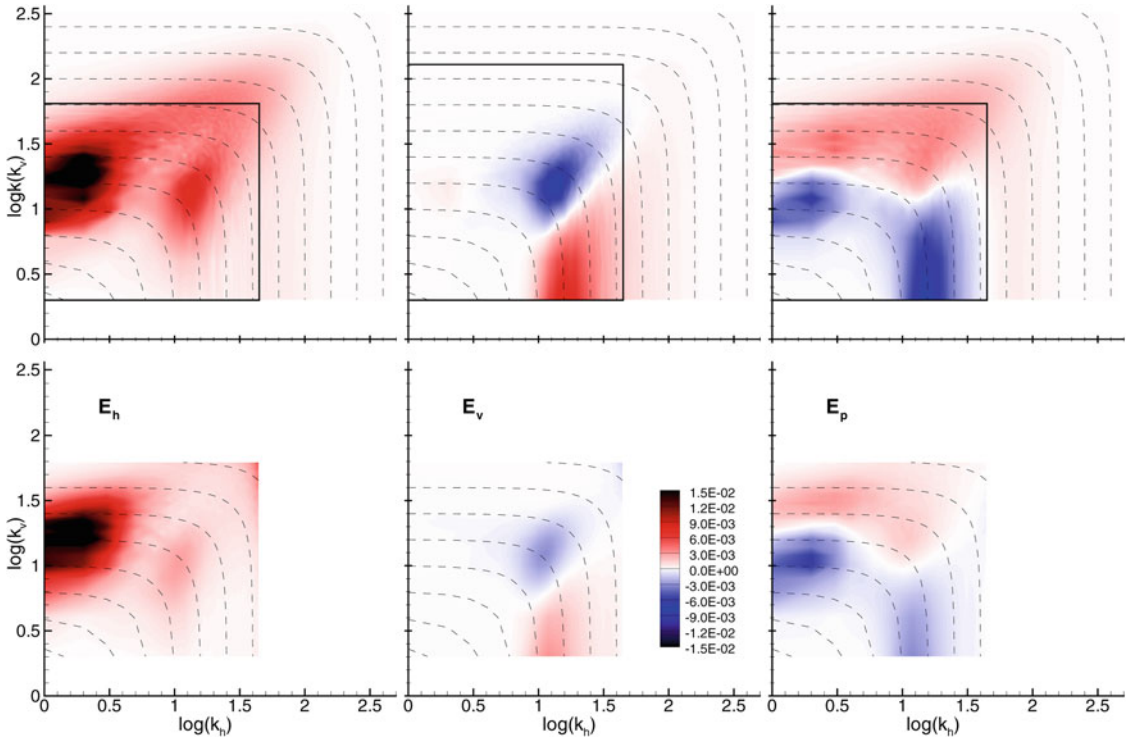


**Fig. 13** Two-dimensional spectra of turbulent diffusion $\widehat{\mathcal{T}}$ in stratified turbulence ($Fr = 0.025$, $Re = 6{,}100$, $\mathcal{R} = 3.7$). DNS (*top row*) and ILES with ALDM (*bottom row*)

Since $\widehat{\mathcal{T}}$ is a pure energy transport term, its integral over all wavenumbers is zero for each individual energy form in the DNS. In the under-resolved ILES, the complete region of negative turbulent diffusion is resolved, but part of the region where it is positive (and energy is dissipated by molecular viscosity) is not included. Hence the integral of $\widehat{\mathcal{T}}$ over the ILES domain must be smaller than zero, corresponding to an effective dissipation of energy. The implicit SGS model automatically accounts for this effect. In the example presented in Fig. 13, the implicit SGS dissipation compared to the total (resolved molecular plus implicit) dissipation amounts to $\mathcal{T}_i(E_h)/\varepsilon_h = 0.63$, $\mathcal{T}_i(E_v)/\varepsilon_v = 0.48$, and $\mathcal{T}_i(E_p)/\varepsilon_p = 0.54$, respectively. About half of the total energy dissipation is provided by the implicit SGS model.

## 5 Conclusion

We presented new results from DNS of horizontally forced homogeneous stratified turbulence of a Boussinesq fluid at different Reynolds and Froude numbers. Our numerical set-up is similar to previous simulations, which allowed us to compare results with literature. In addition to the previously investigated cases, the parameter range of the new DNS data extends to significantly higher buoyancy Reynolds numbers and covers the strongly stratified regime as well as the transition to weak and neutral stratification. We thoroughly discussed two-dimensional spectra for all three forms of flow energy: horizontal and vertical kinetic energy and potential energy. A particular emphasis was put on identifying the mechanisms that govern the conversion of energy and its transport between different scales. This was achieved through analyzing the contributions of all terms of the Boussinesq energy budget equations in spectral space.

Confirming the findings of Brethouwer et al. [5], we observed that the ratio of potential to kinetic energy as well as the mixing efficiency decreases with increasing stratification. In extending previous studies to higher buoyancy Reynolds numbers, we found that both ratios also tend to decrease for very weak stratification, which means that there is a peak at about $10 < \mathcal{R} < 100$.

The horizontal kinetic energy accumulates in modes with high vertical and low horizontal wavenumber ("pancake-turbulence"), while the vertical kinetic energy is distributed much more isotropically in spectral space. The available potential energy distribution combines elements of both kinetic energy types. It has a

strong peak on vertical modes like the horizontal kinetic energy and it has some contribution on medium horizontal scales like the vertical kinetic energy. In analyzing the contributions of the different terms in the energy transport equations to the total energy balance, we could show in detail the various ways in which energy is transformed and transported. Furthermore, we found that with changing Reynolds number the relevant parameter for controlling the distribution of energy in the wavenumber space is the Froude number rather than the buoyancy Reynolds number. We observed similar spectra in simulations with comparable Froude number and strongly varying spectra if the buoyancy Reynolds number was fixed.

To reduce the computational costs of simulating stratified turbulent flows, we proposed an implicit SGS model for LES based on the ALDM [19,21]. In ALDM, the SGS stress term is not explicitly computed based on the available flow solution, but it is rather part of the non-linear numerical discretization. The implicit SGS model provided by this discretization can be interpreted as a combination of tensor dissipation and scale similarity modeling. When applying ALDM to homogeneous stratified turbulence, we found good agreement with the DNS results. ALDM correctly predicts trends and values of integral flow parameters, such as the ratios of different types of energy. Especially in cases of strong stratification, the ALDM predictions are much closer to the DNS results than simulations with a Smagorinsky model. The same observation is made for the prediction of energy spectra. We emphasize that ALDM does neither require ad hoc modifications nor a re-calibration of model parameters. We used the very same set of model parameters for our simulations of stratified turbulence that had been found to be optimal for isotropic neutrally stratified turbulence before. The implicit model automatically adapts to anisotropic conditions and predicts the spectra modified by strong stratification much better than a classical eddy viscosity model.

We conclude that ALDM is a suitable tool for simulating turbulent flows in stably stratified background. The applicability of ALDM to (neutrally stratified) engineering flows had already been shown in a number of previous studies. With the present investigations, we also qualified the implicit SGS model for use in geophysical applications. Future applications of ALDM include breaking of gravity waves, atmospheric boundary layers, mixing events in the ocean and other small and mesoscale phenomena.

**Acknowledgments** This work was funded by the German Research Foundation (DFG) in the framework of the MetStröm priority program. Computational resources were provided by the High Performance Computing Center Stuttgart (HLRS) under the grant TIGRA. The first author gratefully acknowledges the support of the TUM Graduate School's Faculty Graduate Center of Mechanical Engineering at Technische Universität München.

## References

1. Aspden, A.J., Nikiforakis, N., Dalziel, S.B., Bell, J.B.: Analysis of implicit les methods. Comm. App. Math. Comp. Sci. **3**(1), 103–126 (2008)
2. Billant, P., Chomaz, J.M.: Theoretical analysis of the zigzag instability of a vertical columnar vortex pair in a strongly stratified fluid. J. Fluid Mech. **419**(1), 29–63 (2000)
3. Boris, J., Grinstein, F., Oran, E., Kolbe, R.: New insights into large eddy simulation. Fluid Dynam. Res. **10**(4–6), 199–228 (1992)
4. Bouruet-Aubertot, P., Sommeria, J., Staquet, C.: Stratified turbulence produced by internal wave breaking: two-dimensional numerical experiments. Dyn. Atmos. Oceans **23**(1–4), 357–369 (1996). Stratified flows
5. Brethouwer, G., Billant, P., Lindborg, E., Chomaz, J.M.: Scaling analysis and simulation of strongly stratified turbulent flows. J. Fluid Mech. **585**, 343–368 (2007)
6. Cot, C.: Equatorial mesoscale wind and temperature fluctuations in the lower atmosphere. J. Geophys. Res. **106**(D2), 1523–1532 (2001)
7. Dewan, E.M.: Stratospheric wave spectra resembling turbulence. Science **204**(4395), 832–835 (1979)
8. Dewan, E.M.: Saturated-cascade similitude theory of gravity wave spectra. J. Geophys. Res. **102**(D25), 29799–29817 (1997)
9. Diamessis, P.J., Spedding, G.R., Domaradzki, J.A.: Similarity scaling and vorticity structure in high-reynolds-number stably stratified turbulent wakes. J. Fluid Mech. **671**, 52–95 (2011)
10. Domaradzki, J.A., Adams, N.A.: Direct modelling of subgrid scales of turbulence in large eddy simulations. J. Turb. **3**, 24 (2002)
11. Dörnbrack, A.: Turbulent mixing by breaking gravity waves. J. Fluid Mech. **375**, 113–141 (1998)
12. Fritts, D.C., Wang, L., Werne, J., Lund, T., Wan, K.: Gravity wave instability dynamics at high reynolds numbers. part i: wave field evolution at large amplitudes and high frequencies. J. Atmos. Sci. **66**(5), 1126–1148 (2009)
13. Gage, K.S.: Evidence for a $k^{-5/3}$ law inertial range in mesoscale two-dimensional turbulence. J. Atmos. Sci. **36**, 1950–1954 (1979)
14. Grinstein, F.F., Margolin, L.G., Rider, W.J. (eds.): Implicit Large Eddy Simulation—Computing Turbulent Fluid Dynamics. Cambridge University Press, Cambridge (2007)
15. Harten, A., Engquist, B., Osher, S., Chakravarthy, S.R.: Uniformly high order accurate essentially non-oscillatory schemes. III. J. Comput. Phys. **71**(2), 231–303 (1987)
16. Herring, J.R., Métais, O.: Numerical experiments in forced stably stratified turbulence. J. Fluid Mech. **202**(1), 97–115 (1989)

17. Hickel, S., Adams, N.A.: On implicit subgrid-scale modeling in wall-bounded flows. Phys. Fluids **19**, 105–106 (2007)
18. Hickel, S., Adams, N.A.: Implicit les applied to zero-pressure-gradient and adverse-pressure-gradient boundary-layer turbulence. Int. J. Heat Fluid Flow **29**, 626–639 (2008)
19. Hickel, S., Adams, N.A., Domaradzki, J.A.: An adaptive local deconvolution method for implicit LES. J. Comput. Phys. **213**, 413–436 (2006)
20. Hickel, S., Adams, N.A., Mansour, N.N.: Implicit subgrid-scale modeling for large-eddy simulation of passive scalar mixing. Phys. Fluids **19**, 095–102 (2007)
21. Hickel, S., Kempe, T., Adams, N.A.: Implicit large-eddy simulation applied to turbulent channel flow with periodic constrictions. Theor. Comput. Fluid Dyn. **22**, 227–242 (2008)
22. Kaltenbach, H.J., Gerz, T., Schumann, U.: Large-eddy simulation of homogeneous turbulence and diffusion in stably stratified shear flow. J. Fluid Mech. **280**(1), 1–40 (1994)
23. Kawamura, T., Kuwahara, K. (eds.): Computation of high Reynolds number flow around a circular cylinder with surface roughness (1984)
24. Kraichnan, R.H.: Inertial ranges in two-dimensional turbulence. Phys. Fluids **10**(7), 1417–1423 (1967)
25. Laval, J.P., McWilliams, J.C., Dubrulle, B.: Forced stratified turbulence: successive transitions with Reynolds number. Phys. Rev. E **68**(3), 036–308 (2003)
26. Lilly, D.K.: Stratified turbulence and the mesoscale variability of the atmosphere. J. Atmos. Sci. **40**(3), 749–761 (1983)
27. Lilly, D.K., Bassett, G., Droegemeier, K., Bartello, P.: Stratified turbulence in the atmospheric mesoscales. Theor. Comput. Fluid Dyn. **11**, 139–153 (1998)
28. Lindborg, E.: The energy cascade in a strongly stratified fluid. J. Fluid Mech. **550**(1), 207–242 (2006)
29. Lindborg, E., Brethouwer, G.: Stratified turbulence forced in rotational and divergent modes. J. Fluid Mech. **586**, 83–108 (2007)
30. Métais, O., Lesieur, M.: Spectral large-eddy simulation of isotropic and stably stratified turbulence. J. Fluid Mech. **239**, 157–194 (1992)
31. Nastrom, G.D., Gage, K.S.: A climatology of atmospheric wavenumber spectra of wind and temperature observed by commercial aircraft. J. Atmos. Sci. **42**(9), 950–960 (1985)
32. Shu, C.W.: Total-variation-diminishing time discretizations. SIAM J. Sci. Stat. Comput. **9**(6), 1073–1084 (1988)
33. Smith, L.M., Waleffe, F.: Generation of slow large scales in forced rotating stratified turbulence. J. Fluid Mech. **451**(1), 145–168 (2002)
34. Smolarkiewicz, P.K., Margolin, L.G.: MPDATA: a finite-difference solver for geophysical flows. J. Comput. Phys. **140**(2), 459–480 (1998)
35. Staquet, C., Godeferd, F.S.: Statistical modelling and direct numerical simulations of decaying stably stratified turbulence. Part 1. Flow energetics. J. Fluid Mech. **360**, 295–340 (1998)
36. van Zandt, T.E.: A universal spectrum of buoyancy waves in the atmosphere. Geophys. Res. Lett. **9**(5), 575–578 (1982)
37. van der Vorst, H.A.: Bi-CGSTAB: a fast and smoothly converging variant of Bi-CG for the solution of nonsymmetric linear systems. SIAM J. Sci. Stat. Comput. **13**(2), 631–644 (1992)
38. Waite, M.L., Bartello, P.: Stratified turbulence dominated by vortical motion. J. Fluid Mech. **517**, 281–308 (2004)